Scientific paper

Rotating Ring–Disk Electrode with Dual Dynamic Potential Control: Theory and Practice

Soma Vesztergom,[1,3,*] Norbert Barankai,[2] Noémi Kovács,[1] Mária Ujvári,[1] Thomas Wandlowski[3] and Győző G. Láng[1]

[1] *Eötvös Loránd University, Department of Physical Chemistry*

[2] *Eötvös Loránd University, Department of Physics of Complex Systems*

[3] *University of Bern, Department of Chemistry and Biochemistry,*

** Corresponding author: E-mail: vesztergom@chem.elte.hu*
Tel: +36 20 461-2429

Received: 29-01-2014

Paper based on a presentation at the 4th RSE-SEE 2013 Symposium on Electrochemistry in Ljubljana, Slovenia

Abstract

Using the LabVIEW™ graphical programming language designed by National Instruments®, a digital simulation model has been developed in order to describe electrochemical processes occurring at rotating ring–disk electrodes. The model allows for taking into consideration independent potential control of the two working electrodes, homogeneous electrode reactions, as well as spatial inhomogeneities of the working electrode surfaces. The main programming concepts, as well as the operation of the simulation software is presented. Several test simulations have been carried out in order to evaluate the accuracy of the calculations.

Keywords Rotating ring–disk electrode, electrochemistry, digital simulations, dual potentiodynamic control

1. Introduction

The LabVIEW™ graphical programming language designed by National Instruments® has gained wide popularity in every scientific field where the quality of the results highly depends on the level of automation of the measurements[1]. For instance, some earlier papers of the present authors have demonstrated that with the application of the state-of-the-art graphical programming techniques offered by LabVIEW, significant improvements can be made to increase the sensitivity and the range of applicability of electrochemical techniques based on the use of rotating ring–disk electrodes (RRDEs)[2–6].

In the present paper it will be demonstrated that LabVIEW might not only be used for the automation of RRDE measurements, but it also provides straightforward means for simulating such experiments. This makes the direct comparison of experimental results and theoretical predictions possible within the same software environment.

1. 1. Rotating Ring–Disk Electrodes

Rotating ring–disk electrodes are well-known and commonly used devices of investigating electrode reaction mechanisms. The rotating ring–disk electrode (Figure 1) consists of two metal parts: the disk, and the electrically separated ring that concentrically surrounds it.

If on the generator (disk) electrode some electroactive species are formed as a result of an electrode reaction, these species will be swept away by the convection arising from the rotation of the electrode to the collector (the ring). At the ring electrode, if its potential is suitably chosen, the arriving electroactive species can be "collected" – that is, they might undergo another electrode reaction, thereby causing changes in the measured ring current.

The RRDE is a very powerful tool of studying homogeneous and heterogeneous kinetics,[7–8] determining diffusion coefficients,[9] investigating corrosion,[10–11] oxygen reduction,[12] electrodeposition,[13] and many other phenomena. The basics of the RRDE technique are discussed

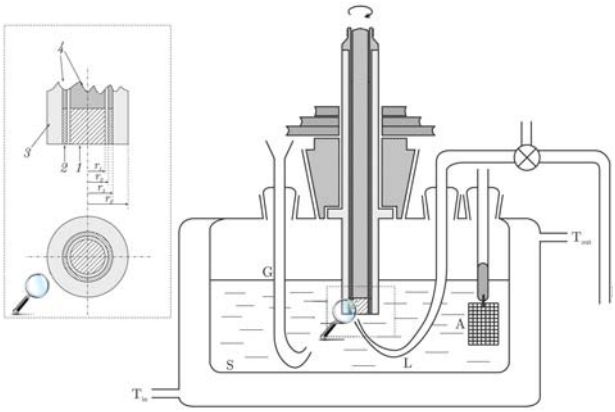

Figure 1: Schematic view of an electrochemical cell with a rotating ring–disk electrode (shown in the inset). ***Parts of the cell* – G:** gas inlet, $\mathbf{T_{in}}$ and $\mathbf{T_{out}}$: in- and outlets for the thermostating fluid, **S:** solution, **L:** Luggin-probe, **A**: auxiliary electrode, **R**: reference compartment. ***Parts of the RRDE – 1:*** disk electrode material, ***2:*** ring electrode material, ***3:*** insulator, ***4:*** metal support, r_1: disk radius, r_2: inner ring radius, r_3: outer ring radius, r_0: overall radius of the tip.

in most electrochemistry textbooks,[14–15] but a few handbooks[16–17] are dedicated to the topic as well.

Like many other surveys based on the use of two working electrodes, RRDE experiments involve the examination of two potentials (E_{disk} and E_{ring}) and two currents (I_{disk} and I_{ring}). The representation of the results thus involves more dimensions than that of usual electrochemical measurement results obtained from a single working electrode only[14]. The most common techniques of using an RRDE are as follows:

– A current-potential curve is recorded at the disk while the ring potential is held at a constant value where the intermediates or products are reduced or oxidized. This allows the identification of the exact potential range over which the products are formed.
– The disk can be held at a potential where intermediates or products are formed, while maintaining the ring potential also at a constant value at which the products are electro-active.
– While holding the disk at a potential where the reaction of interest takes place, a current-potential curve can be obtained from the ring. This allows the identification of intermediates and/or products.
– The subject of observation can also be the transient shielding of the ring current for the electrolysis of a species upon stepping the disk potential to a value where this species is adsorbed.

Although the most significant advantage of RRDE measurements, compared to those involving quiescent electrodes, is the ability to make measurements at steady state without the need of considering the time of electrolysis, the observation of current transients at the disk or ring can sometimes also be of use in electrochemical investigations. In addition, it has been shown in the recent past[2–6] that the simultaneous application of dual dynamic perturbations to the disk and the ring (that is, the application of "transient techniques" at both working electrodes) is also a useful approach for the elucidation of electrode reaction kinetics – especially the method of dual cyclic voltammetry[3,5] seems to be a very promising technique.

Nevertheless, there still exist a lot of theoretical and practical problems concerning these techniques, which still need to be addressed. Here we devise a digital simulation approach, which based on the classical finite-element

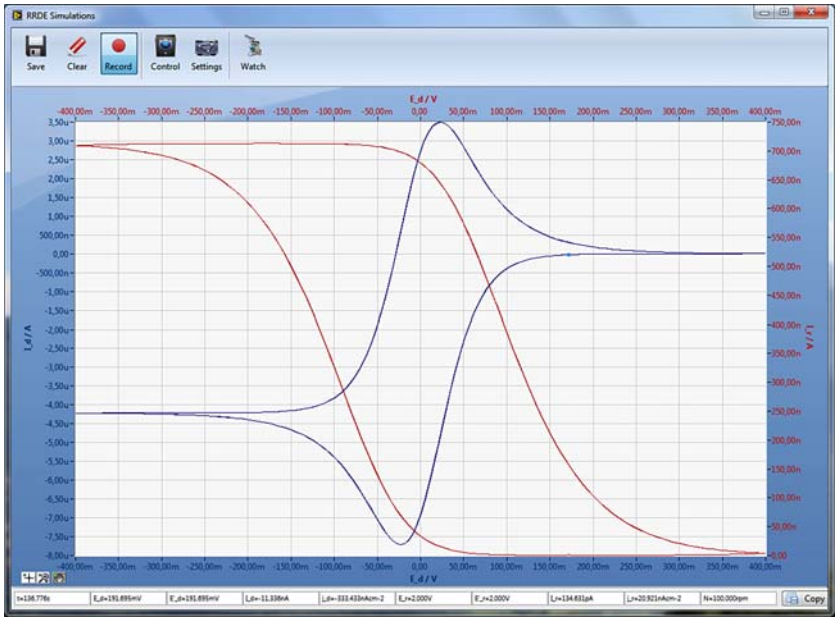

Figure 2: The graphical user interface of the software designed in LabVIEW for the simulation of RRDE experiments.

methods (similar to those described in[18–20]) can be used in order to model

– charge transfer processes occurring at the disk and ring electrodes of an RRDE at the same time, when the electrode potentials of the two electrodes are varied in an arbitrarily time-dependent way;
– mass transfer processes taking place under the rotating ring–disk electrode by means of diffusion and convection;
– homogeneous chemical reactions occurring in the solution.

The operation and design concepts of the simulation software (Figure 2), created in the LabVIEW development environment shall be described in details.

2. Theory

The calculations presented in this paper are confined to a system which contains two given species (denoted with Red and Ox), and in which these electroactive species can undergo the electrode reaction

$$Ox + e^- \rightleftarrows Red \quad (1)$$

at the two electrode surfaces; the direction and rate of the reaction depends on the respective (disk or ring) electrode potential.

We assume that the system can be described *i.)* by taking into consideration charge transfer effects (the reaction according to equation 1 occurring at the disk and ring electrode surfaces, obeying the Erdey-Grúz–Volmer mechanism); *ii.)* by assuming that mass transfer takes place by means of diffusion and convection only (it is assumed that the system contains a supporting electrolyte in a high enough concentration, thus the role of migration can be neglected); and *iii.)* by taking into account homogeneous chemical reactions occurring in the bulk solution.

2. 1. The Simulation Framework

For deriving the simulation algorithm, the cylindrical symmetry of the RRDE system has been fully exploited (Figure 3). The concentration and flow velocity distribution under the RRDE was assumed to be a function of two variables, the distance r measured from the rotation axis and the distance z measured from the electrode surface.

The method of finite volumes has been used in order to carry out the simulations: with planes parallel to the electrode surface, the solution space was divided into layers, and these layers were further divided into cylinders, the symmetry axis of which was the axis of rotation.

The spatial discretization was made "smooth" enough, so that the variables could be considered homogeneous inside of each cell within a Δt time-step of the simulation. As it can be seen in Figure 2, a non-uniform tiling was chosen. In Figure 2 one can note *i.*) that the distances between the horizontal grid lines are growing exponentially with the distance measured from the electrode surface (due to the fact that at places further away from the electrode, the concentrations are expected to change less rapidly as in the vicinity of the metal surface); and *ii.)* that the vertical grid lines are placed in such a way that an appropriately dense tiling appears under the ring electrode as well (the ring has a thickness smaller than the radius of the disk, thus a finer tiling is required here).

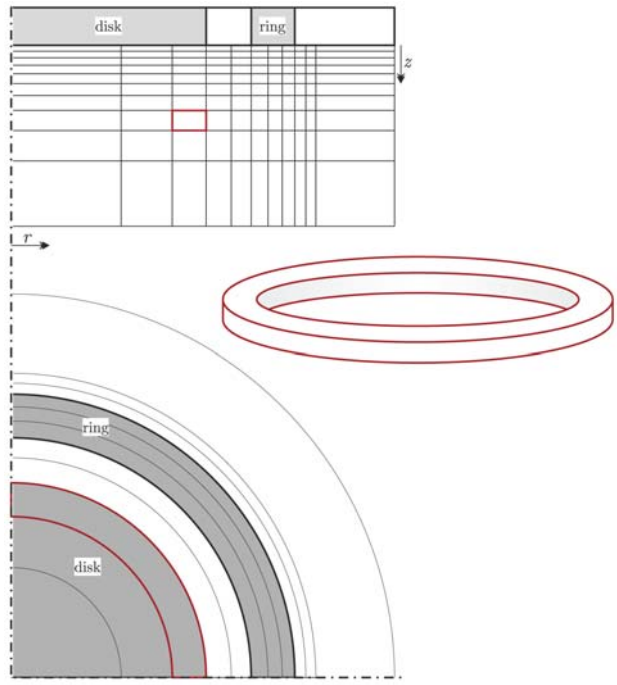

Figure 3: The simulation grid is created by tiling the space below the RRDE into small annulus-shaped cells. An arbitrarily chosen cell is shown "in perspective". This kind of spatial discretization relies heavily on the axial symmetry of the system. The spatial coordinates r and z are shown in the figure.

It was found that in order to obtain well-behaved simulation results, the *vertical spread* of the simulation grid should exceed three or four times the maximal diffusion layer thickness defined as

$$\delta_{max} \approx 1.61 D_{max}^{1/3} \nu^{1/6} \omega^{-1/2} \quad (2)$$

(by Bard and Faulkner,[14] section 9.1), where D_{max} is the highest diffusion coefficient present in the system, ν is the kinematic viscosity of the solution and ω is the rotation rate (more precisely, angular frequency) of the RRDE.

The *horizontal spread* of the simulation grid was set large enough, so that it significantly exceeded the radius of the ring electrode.

As a consequence of the spatial discretization described here, it became possible to treat the simulation va-

Table 1: Some parameters of a simulation cell (like the one shown in Figure 2) that are used in the calculations.

Parameters	Definition
$r^{(j,k)}$ and $z^{(j,k)}$	Radial and axial coordinates of the center of the $(j, k)^{th}$ cell.
$\Delta r^{(j,k)}$ and $\Delta z^{(j,k)}$	Width and height of the $(j, k)^{th}$ cell.
$V^{(j,k)}$	Volume of the $(j, k)^{th}$ cell
$A_{bas}^{(j,k)}$	Area of the top (or equivalently, bottom) bounding surface of the $(j, k)^{th}$ cell.
$A_{int}^{(j,k)}$ and $A_{ext}^{(j,k)}$	Inner and outer bounding surface areas (respectively) of the $(j, k)^{th}$ cell.
$d_{int}^{(j,k)}$, $d_{sup}^{(j,k)}$	Distances measured between the center of the inner, upper, outer and lower neighbours
$d_{ext}^{(j,k)}$ and $d_{inf}^{(j,k)}$	and the center of the $(j, k)^{th}$ cell.
$v_r^{(j,k)}$ and $v_z^{(j,k)}$	Vector components of the $\boldsymbol{v}$ flow velocity at the center of the $(j, k)^{th}$ cell.

riables as two-dimensional arrays in the software (with indices (j, k) standing for rows and columns, respectively). Some parameters corresponding to the simulation cells are listed in Table 1.

Naturally, the smoothness of the grid has to be set fine enough in order to gain accurate results; however it should be noted that since the horizontal and vertical spreads are fixed (as described above), increasing the smoothness of the grid leads to the creation of bigger arrays, and ultimately, longer computation times. The computation time is further elongated by the fact that the simulation time step Δt has to be sufficiently small, so that for each cell with indices (j, k), Δt meets the following requirement:

$$\Delta t \le \min\left\{\frac{\Delta r^{(j,k)^2}}{D_{max}}, \frac{\Delta z^{(j,k)^2}}{D_{max}}, \frac{\Delta r^{(j,k)}}{v_r^{(j,k)}}, \frac{\Delta z^{(j,k)}}{v_z^{(j,k)}}\right\}. \quad (3)$$

The simulation process is started from an arbitrarily chosen set of the variables (practically from a uniform distribution of c_{Red} and c_{Ox}). In each step of the iteration, we first realize the boundary conditions dictated by the charge transfer kinetics at the disk and ring electrode surfaces (this changes the concentrations in each simulation cell that is neighbouring either one of the two electrodes); and then calculate the mass transfer effects that the concentration changes of the boundary cells initiate in the system. In the meantime, we must also account for the concentration changes introduced to the system by homogeneous kinetics. The simulation process is described below in details.

2. 2. Calculations Related to Charge Transfer

Charge transfer only has an effect on those cells, in the first row of the simulation grid, which are neighbouring either the disk or the ring. Based on the Erdey-Grúz–Volmer-mechanism, the current passing into these cells (marked with indices $(0, k)$) can be given as

$$I_{EV}^{(0,k)} = FA_{bas}^{(0,k)}k\left(c_{Red}^{(0,k)}\exp\left[\frac{\alpha F\left(E-E^{\Theta}\right)}{RT}\right] - c_{Ox}^{(0,k)}\exp\left[\frac{(\alpha-1)F\left(E-E^{\Theta}\right)}{RT}\right]\right), \quad (4)$$

where k is the rate constant, α the transfer coefficient and E^{Θ} the standard potential of the electrode reaction described by equation 1, and E is the respective (disk or ring) electrode potential.[14]

Although it would be possible to determine the concentration changes in these cells by using a finite difference approximation of the form

$$\Delta c = \frac{I_{EV}^{(0,k)}\Delta t}{FV^{(0,k)}}, \quad (5)$$

it was found that this approach (especially if the current $I^{(0,k)}{}_{EV}$ or the time step Δt is big) is often erroneous, and results in negative concentration values. According to the literature,[21] the usual approach used in such cases would be the application of Nernstian boundary conditions, which however does not allow for the introduction of charge transfer limitations to the system.

As an alternative way, we have expressed the integral of equation 4 analytically, and based on this expression we found that the new concentration values in each cell ($c'^{(0,k)}$) can be calculated from the old ones ($c'^{(0,k)}$) based on the following equations:

$$c'^{(0,k)}_{Ox} = \frac{b\Sigma c^{(0,k)} + \left(c_{Ox}^{(0,k)} - bc_{Red}^{(0,k)}\right)\exp\left[-\frac{(b+1)\left(b^{\alpha-1}k\Delta t\right)}{\Delta z^{(0,k)}}\right]}{b+1}, \quad (6.a)$$

and

$$c'^{(0,k)}_{Red} = \frac{\Sigma c^{(0,k)} + \left(bc_{Red}^{(0,k)} - c_{Ox}^{(0,k)}\right)\exp\left(-\frac{(b+1)\left(b^{\alpha-1}k\Delta t\right)}{\Delta z^{(0,k)}}\right)}{b+1}. \quad (6.b)$$

In equations 6.a–6.b, $\Sigma c^{(0,k)}$ is the (constant) sum of $c^{(0,k)}{}_{Ox}$ and $c^{(0,k)}{}_{Red}$ in the given cell; and the dependence on the electrode potential is introduced through the variable b defined as

$$b = \exp\left[\frac{F\left(E-E^{\Theta}\right)}{RT}\right]. \quad (7)$$

The electrical current yielded by each cell can then be obtained as

$$I^{(0,k)} = \frac{F V^{(0,k)} \left(c'^{(0,k)}_{\mathrm{Ox}} - c^{(0,k)}_{\mathrm{Ox}} \right)}{\Delta t}, \tag{8}$$

and by carrying out the summation

$$I_{\mathrm{electrode}} = \sum_k I^{(0,k)} \tag{9}$$

for all the cells neighbouring the electrode in question, the net current of the electrode can be determined.

As opposed to the finite difference-based approximation of equation 5, the strategy presented here was found suitable for determining concentration changes caused by charge transfer effects, even if the system was far away from equilibrium. Later in Section 3.1, the validity of the calculations will be tested by the comparison of simulated data with some theoretical expectations.

2. 2. 1. Electrodes with Inhomogeneous Surface Activity

Naturally, when carrying out the calculations for a cell in the vicinity of one of the electrodes (equations 6–8), the values of k, E and α should be those corresponding to the electrode in question (that is, the disk or the ring, respectively). It should also be noted, however, that the values of k and α should not necessarily be constant over the whole area of an electrode[20]. Simulations may also be performed by assuming that these values change from cell to cell (meaning that instead of handling them as global constants, we use $k^{(k)}$ and $\alpha^{(k)}$ as indexed variables). By using this approach, our model is suitable to describe processes occurring at electrode surfaces with a (spatially) inhomogeneous catalytic activity.

2. 3. Calculations Related to Processes in the Bulk Phase

If we assume that owing to a high supporting electrolyte concentration the effect of migration is negligible, the transport of a species i in the RRDE system can be treated as result of a joint influence of diffusion and convection effects. The transport processes (as well as the effects of homogeneous reactions) can be described reasonably well by a discretization of the general transport equation over the simulation grid in the form

$$\begin{aligned} c'^{(j,k)}_i = c^{(j,k)}_i + \frac{\Delta t\, D_i}{V^{(j,k)}} \Bigg(& \frac{A^{(j,k)}_{\mathrm{int}} \left(c^{(j,k-1)}_i - c^{(j,k)}_i \right)}{d^{(j,k)}_{\mathrm{int}}} + \\ & + \frac{A^{(j,k)}_{\mathrm{bas}} \left(c^{(j,k-1)}_i - c^{(j,k)}_i \right)}{d^{(j,k)}_{\mathrm{sup}}} + \frac{A^{(j,k)}_{\mathrm{ext}} \left(c^{(j,k-1)}_i - c^{(j,k)}_i \right)}{d^{(j,k)}_{\mathrm{ext}}} + \\ & + \frac{A^{(j,k)}_{\mathrm{inf}} \left(c^{(j,k-1)}_i - c^{(j,k)}_i \right)}{d^{(j,k)}_{\mathrm{inf}}} \Bigg) \\ & + \frac{\Delta t\, v^{(j,k)}_r \left(c^{(j,k-1)}_i - c^{(j,k)}_i \right)}{d^{(j,k)}_{\mathrm{int}}} + \frac{\Delta t\, v^{(j,k)}_z \left(c^{(j,k-1)}_i - c^{(j,k)}_i \right)}{d^{(j,k)}_{\mathrm{inf}}} \end{aligned} \tag{10}$$

that is, as a sum of four diffusion-related, two convection-related and some chemical terms. Equation 10 is readily usable in explicit simulations, provided that the vector components v_r and v_z of the flow velocity field are known at the centre of each cell, and that the kinetic equations of the homogeneous reactions are known and may be accounted for.

2. 3. 1. Determining the Velocity Profile $v(r,z)$

In order to describe fluid flow under a rotating disk, the classical approach devised by Kármán has been followed (see the original paper[22] as well as an excellent review[23] of this matter). The Navier–Stokes equations governing fluid flow in the rotating disk system were solved by using the same simplifications that Kármán has introduced.

The Navier–Stokes equations for an incompressible fluid and the equation of continuity can be written in general as

$$\frac{\mathrm{d}\boldsymbol{v}}{\mathrm{d}t} = -\mathrm{grad}\,\frac{p}{\rho} + \nu\,\mathrm{div}\,\mathrm{grad}\boldsymbol{v} + \frac{\boldsymbol{f}}{\rho}, \tag{11.a}$$

and

$$\mathrm{div}\,\boldsymbol{v} = 0. \tag{11.b}$$

Relying on the simplifications introduced by Kármán*, equations 11.a–11.b can be expressed in the following form using cylindrical coordinates:

$$v_r \frac{\partial v_r}{\partial r} + v_z \frac{\partial v_r}{\partial z} - \frac{v_\varphi^2}{r} = \nu \left[\frac{\partial^2 v_r}{\partial r^2} + \frac{\partial}{\partial r}\left(\frac{v_r}{r} \right) + \frac{\partial^2 v_r}{\partial z^2} \right] \tag{12.a}$$

$$v_r \frac{\partial v_\varphi}{\partial r} + v_z \frac{\partial v_\varphi}{\partial z} + \frac{v_r v_\varphi}{r} = \nu \left[\frac{\partial^2 v_\varphi}{\partial r^2} + \frac{\partial}{\partial r}\left(\frac{v_\varphi}{r} \right) + \frac{\partial^2 v_\varphi}{\partial z^2} \right] \tag{12.b}$$

$$v_z \frac{\partial v_z}{\partial z} = -\frac{1}{\rho}\frac{\partial p}{\partial z} + \nu \frac{\partial^2 v_z}{\partial z^2} \tag{12.c}$$

$$0 = \frac{\partial v_r}{\partial r} + \frac{v_r}{r} + \frac{\partial v_z}{\partial z} \tag{12.d}$$

In case of a rotating disk, the boundary conditions of the system of partial differential equations 12.a–12.d can

* The assumptions of Kármán include *i.)* that we only deal with non-turbulent stationary flow, when $\partial \boldsymbol{v}/\partial t = 0$; *ii.)* that due to the axial symmetry of the system, $\partial \boldsymbol{v}/\partial \varphi = 0$; *iii.)* that the axial component of the velocity vector is independent from the radial coordinate ($\partial v_z/\partial r = 0$); *iv.)* that we consider the density ρ constant and the pressure p being dependent of z, but not of r or φ; and *v.*) that we assume that no natural forces act on the system ($\boldsymbol{f} = 0$).

be formulated as

$$v_r = 0 \qquad v_\varphi = \omega r \qquad v_z = 0 \qquad \text{at } z = 0,$$

$$v_r = 0 \qquad v_\varphi = 0 \qquad v_z = \text{constant} \qquad \text{at } z = \infty;$$

i.e., we assume that near the rotating surface no slip occurs (the fluid moves together with the disk), while far away from the rotating surface, the axial component of the fluid flow is of constant value while the radial and angular components are both zero.

By introducing the dimensionless variable $\gamma = z\sqrt{\omega/\nu}$, as well as the substitutions

$$v_r = r\omega F(\gamma), \tag{13.a}$$

$$v_\varphi = r\omega G(\gamma), \tag{13.b}$$

$$v_z = \sqrt{\omega\nu}\, H(\gamma), \tag{13.c}$$

$$p = -\rho\nu\omega P(\gamma), \tag{13.d}$$

the system of partial differential equations 13.a–13.d can be cast into a system of ordinary differential equations

$$2F + \frac{\mathrm{d}H}{\mathrm{d}\gamma} = 0, \tag{14.a}$$

$$H\frac{\mathrm{d}F}{\mathrm{d}\gamma} - G^2 = \frac{\mathrm{d}^2F}{\mathrm{d}\gamma^2}, \tag{14.b}$$

$$2FG + H\frac{\mathrm{d}G}{\mathrm{d}\gamma} = \frac{\mathrm{d}^2G}{\mathrm{d}\gamma^2}, \tag{14.c}$$

$$2\left(FH - \frac{\mathrm{d}F}{\mathrm{d}\gamma}\right) = \frac{\mathrm{d}P}{\mathrm{d}\gamma}. \tag{14.d}$$

It can be easily noted that the function $P(\gamma)$ appears in equation 14.d only, which can thus be decoupled from the system of differential equations. The boundary conditions are as follows:

$$F(0) = 0 \tag{15.a}$$

$$G(0) = 0 \tag{15.b}$$

$$H(0) = 1 \tag{15.c}$$

$$\lim_{\gamma\to\infty} F(\gamma) = 0 \tag{15.d}$$

$$\lim_{\gamma\to\infty} G(\gamma) = 0 \tag{15.e}$$

The usual approach (see Cochran[24] cited by Riddiford[23]) used to solve the system of ordinary differential equations 14.a–14.c with respect to the boundary conditions 15.a–15.e is to look for the solutions in a form of series expansions. For example it was shown[20,23] that the function $H(\gamma)$ can be well approximated for small values of γ in the form

$$H(\gamma) = -0.5102\gamma^2 + \frac{\gamma^3}{3} - 0.1026\gamma^4 + \\ + 0.0126\gamma^5 + \mathcal{O}(6), \tag{16.a}$$

while for higher values of γ, $H(\gamma)$ can be well estimated asymptotically[23] with an exponential series of the form

$$H(\gamma) = -0.89 + 2.1\exp[-0.89\gamma] + \ldots \tag{16.b}$$

It is of worth noting that the level of approximation used in the simulation of RRDE experiments highly differs in the literature. Prater and Bard[18] used only the second order approximation when formulating the first RRDE simulation system; moreover, they have accepted as initial condition that the concentration distribution below the disk is independent of the radius *r*. Thus their approach suffered from significant computation errors necessitating the introduction of "correction factors" that were rather difficult to justify. The method developed by Kiss *et al.*[20] has successfully overcome this problem by applying a radial tiling also below the disk electrode and by using a third order approximation of the series given in equation 16.a.

It was shown later that if further terms of equation 16.a are taken into consideration[25] for estimating the flow velocity profile under the RRDE, an even higher accuracy can be obtained. However, it was also found that for digital simulation purposes (which are, *per se*, numerical methods), finding a solution in a form of power series is highly obsolete. Instead, we followed the so-called "shooting method" by implementing in LabVIEW the algorithm originally developed by Higgins and Binous[27] for Wolfram Research© Mathematica™. That is, in lieu of a full set of initial conditions, we started with estimating the values of $\mathrm{d}F/\mathrm{d}\gamma$ and $\mathrm{d}G/\mathrm{d}\gamma$. Based on these estimates, we solved equations 14.a–14.c in a fully explicit (numerical) way, and then checked for the validity of the boundary conditions 15.d–15.e. In case these conditions (when using a large value of γ instead of the limit $\gamma \to \infty$) were not fulfilled, the initial values of $\mathrm{d}F/\mathrm{d}\gamma$ and $\mathrm{d}G/\mathrm{d}\gamma$ were modified in such a way that the error of the solution would be lowered in the next iteration step.

By the use of this method, the accuracy of determining $F(\gamma)$, $G(\gamma)$ and $H(\gamma)$ could be set arbitrarily high within the domain of the numerical precision used for the simulations (the error could be reduced down to the range of the machine epsilon).

In Figure 4, the curve of the numerically determined $H(\gamma)$ function is presented, together with its approxima-

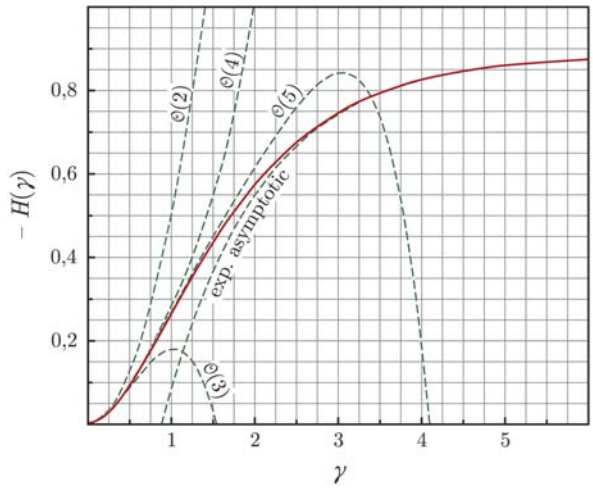

Figure 4: $H(\gamma)$ function values obtained by a numerical solution of the system of ordinary differential equations 14.a–14.c. The solution (solid line) is in agreement with the boundary conditions 15.a–15.e. Different approximations, based on the series expansion 13.a and the asymptote 13.b, are also depicted with dashed lines. The $\mathcal{O}(2)$ and $\mathcal{O}(3)$ series approximations have been used in numerical simulations by Bard and Prater[18], and by Kiss *et al.*[20], respectively.

tions based on equations 16.a–16.b. It can well be seen in Figure 4, that the series approximations based on equation 16.a (which were, nevertheless, used in some digital simulation models) only gave accurate values for indeed small values of γ, while the asymptotic approximation is only accurate for high γ values.

2. 3. 2. The Simulation of Homogeneous Kinetics

As it was mentioned before, our simulation approach is also capable of taking homogeneous chemical reactions occurring in the bulk solution into account. This can be achieved either by using a finite-difference approximation (by adding chemical terms to equation 10), or by using analytical expressions.

In practice, usually the latter option is used, as analogously to the case of charge transfer, the finite difference estimation often results in computational errors. A common approach[20] is to incorporate the simulation of chemical reactions into the bulk transport simulations in an *a posteriori* way; that is, first we calculate the transport effects, and then – based on an analytical solution of the kinetic equations – we calculate the new concentration values which result from the chemical reaction.

3. Test Simulations

In this section, the features of our newly developed simulation system will be demonstrated by various test runs, the results of which are comparable to theoretical (analytical) expectations.

3. 1. Test Simulations with a Single, Stagnant (Disk) Electrode

The effectiveness of the calculation of diffusion was checked by simulating a potential step experiment on the disk electrode. For these calculations, the rotation rate of the electrode was set to 0 min^{-1}, and in a solution containing only the Red species at $t = 0$, the disk electrode potential was set to a very positive value. The simulation results shown in Figure 5 were found to be very close to the theoretical predictions of the Cottrell-equation.

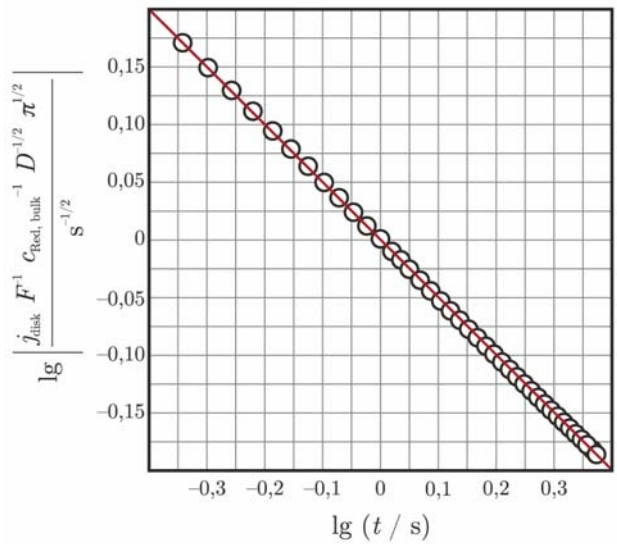

Figure 5: Simulated values of the disk electrode's (transformed) current in a potential step experiment (dots), and the values expected on the basis of the Cottrell-equation. In this particular representation, the results should fit on a line with an intercept of 0 and a slope of –½ (shown with red in the figure).

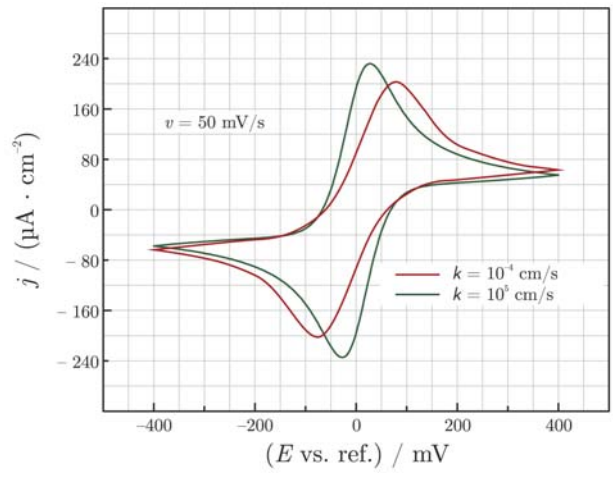

Figure 6: Cyclic voltammograms simulated for a stagnant disk electrode with two different values of the rate constant k. The cyclic voltammograms show a good agreement with the theoretical expectations[14].

In another experiment, cyclic voltammograms were simulated for a stagnant disk electrode in a solution containing both the Red and the Ox species in an equal concentration. Figure 6 shows the simulated CVs in a reversible ($k = 10^5$ cm/s) and in a "quasi-reversible" ($k = 10^{-4}$ cm/s) case. The simulated curves are in a good agreement with the theoretical expectations[14].

3. 2. Test Simulations of Steady-State Collection Experiments at an RRDE

The accuracy of our convection-related calculations was tested by carrying out simulations under the following circumstances:

- it was assumed that at $t = 0$, the system contains the Ox species only (at a given concentration), but no Red is present in the system;
- the disk electrode potential was set negative enough, so that at the disk electrode, arising from the reduction of Ox, a limiting current could be measured;
- the ring electrode potential was in turn set very positive, so that every disk-generated Red species reaching the ring would immediately be oxidized back to Ox.

In this case it was assumed that no homogeneous chemical reaction can takes place in the system. Figure 7 shows that the disk current density values were in a very good agreement with the predictions of the Levich-equation of the form

$$j_{\text{disk}} = 0.62\, F\, D_{\text{Ox}}^{2/3}\, \omega^{1/2}\, \nu^{-1/6}\, \omega^{1/2} c_{\text{Ox, bulk}}, \qquad (17)$$

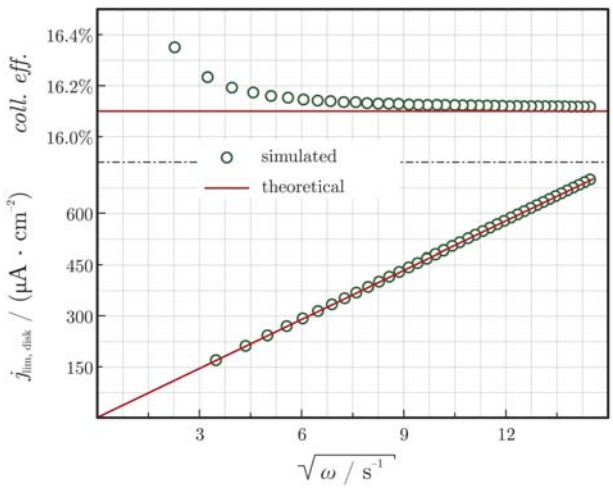

Figure 7: Simulation results from a "steady-state collection" experiment. The disk current densities follow the Levich-equation (lower part of the figure), while the simulated collection efficiencies are very close to their theoretical value (see Bard and Faulkner,[14] section 9.4.2 for more details).

and that the collection efficiency (that is, the $-I_{\text{ring}}/I_{\text{disk}}$ ratio) agrees within a range of per mils with the theoretically expected value (determined as described by Bard and Faulkner,[14] section 9.4.2).

3. 3. Test Simulations of Dual Cyclic Voltammetry at an RRDE

The method of dual cyclic voltammetry has previously been used[3,5] in order to investigate the oxygen reduction process at the (polycrystalline) Au|0.5 mol/dm^3 H_2SO_4 electrode. The application of this method involved the simultaneous recording of a slow-rate linear sweep voltammogram at the disk and high-rate cyclic voltammograms at the ring electrode. It was demonstrated[3] that based on this technique, a "3D map" showing the side products of the disk electrode reaction can be constructed. Such a "3D map" may become useful if one has to determine at which disk potential some electroactive species are formed, and at which ring potential these might be detected.

However, the application of this method brings up a few questions that should be theoretically addressed. For instance, a clear distinction needs to be made in case of such experiments between ring signals arising from an actual collection of a disk-generated species and ring signals which may be caused by products formed earlier (at another E_{ring} value) on the ring electrode itself. Here we demonstrate by the simulation of dual potentiodynamic experiments that setting a high enough rotation rate is invaluable to overcome this issue, since at high angular frequencies the detection of self-generated species at the ring electrode is far less predominant than the collection of disk-generated products.

In order to carry out the simulations, the following assumptions have been made:

- it was assumed that at $t = 0$, the system contains the Ox species only (at a given concentration), but no Red is present in the system;
- it was further assumed that the electrode reaction at both electrodes is fast ($k = 10^4$ cm/s);
- it was assumed that the species Red, if formed, undergoes a first-order decay in the bulk phase with a rate constant of $k_{\text{decay}} = 1$ /s.

In Figure 8, the simulation results carried out at two different rotation rates (100 and 500 min^{-1}) are shown. The upper curves show the disk electrode's LSV response – on these curves, the limiting current is that predicted by equation 17 (the Levich equation). The curves in the lower parts of the figure are cyclic voltammograms measured on the ring at a high sweep-rate (recorded in parallel with the LSV curves of the disk). Like in case of the measurement results presented in our earlier publications[3], it is visible that the shape of the ring CVs change with E_{disk}; the fingerprints of collection (anodic parts) and shading (cathodic parts) can both be seen at rotation rates of 100 and

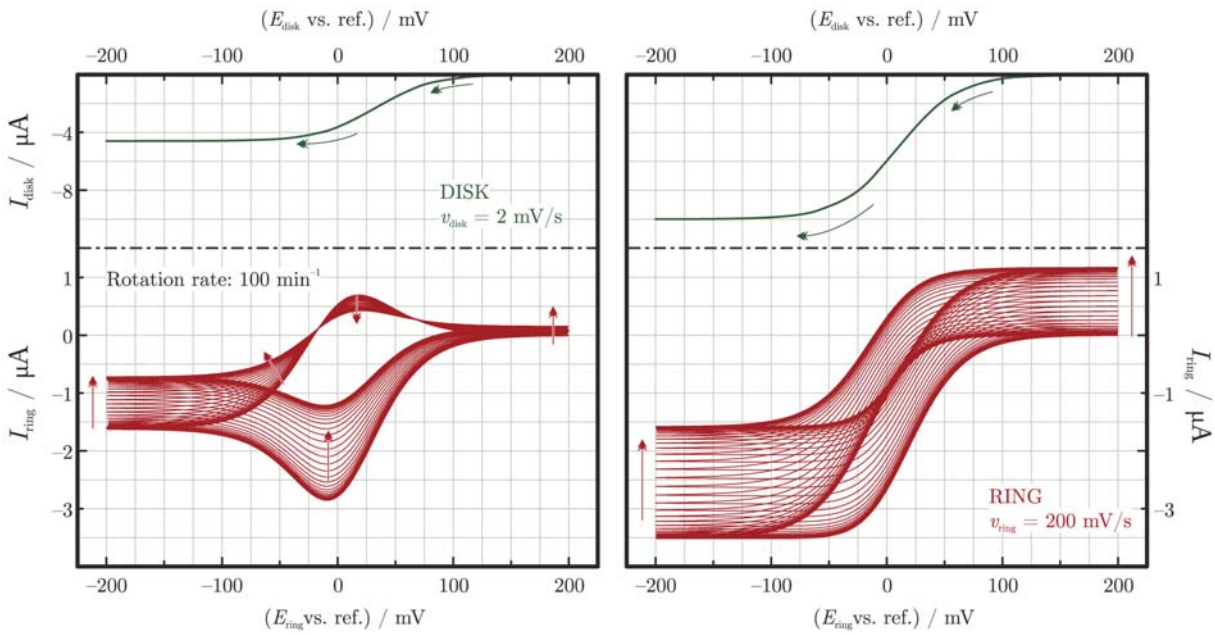

Figure 8: Low-rate linear sweep voltammograms (2 mV/s) and high-rate cyclic voltammograms (200 mV/s) recorded at the disk and ring electrodes, respectively at two different rotation rates (100 and 500 min^{-1}). The measurements made at high rotation rates are free of "self-generated" species collection effects.

500 min^{-1}. However, it should also be noted that at low rotation rates (100 min^{-1}) the reoxidation of self-generated reduction products at the ring may still occur (see the hysteresis of the ring CVs). This effect, even though the sweep rate of the ring is still high, is not experienced at higher rotation rates, when "the rapid convection has enough time" to clear any self-generated products away from the ring surface.

An important result of these simulations is that they are able to show which v_{ring} and ω values are safe to be used in a dual voltammetric RRDE experiment (like those presented in[3,5]), if the detection of self-generated ring products is to be avoided.

4. Conclusions

A new digital simulation approach to the rotating ring–disk electrode system has been devised and documented. As shown by the presented test results, the software can be used in order to simulate RRDE experiments with a very high numerical accuracy. Moreover, the simulation of measurements based on the dual potentiodynamic perturbation of the disk and ring electrodes[1–6] is also possible based on the presented method. This fact offers the possibility of comparing measurement results with theoretical expectations.

As the method allows for the simulation of electrode processes at catalytically inhomogeneous metal | electrolyte solution interfaces, as well as the incorporation of migration and *IR*-drop effects into the model, future work will consider local current distributions at the electrode surfaces and interferences that may arise between the current-potential characteristics of the two working electrodes, due to the finite ohmic resistance of the solution.

5. Acknowledgements

S. Vesztergom gratefully acknowledges the support of the European Union and the State of Hungary, as well as the co-financing of the European Social Fund in the framework of TÁMOP 4.2.4. A/1-11-1-2012-0001 'National Excellence Program'. S. Vesztergom further acknowledges the support of Scientific Exchange Programme NMS^{ch} (SciEx 13.060) for funding his internship at the University of Bern.

N. Barankai gratefully acknowledges the financial support from the grant TÁMOP-4.2.2.c-11/1/konv-2012-0013.

G.G. Láng gratefully acknowledges support from the Hungarian Scientific Research Fund (grants OTKA-K109036, OTKA-67994/ OMFB-01078/2007).

6. References

1. G. W. Johnson, *LabVIEW Graphical Programming: Practical Applications in Instrumentation and Control*, McGraw–Hill, New York, 2007.
2. S. Vesztergom, M. Ujvári, G. G. Láng, *Electrochem. Comm.* **2011**, *13*, 378–381.

3. S. Vesztergom, M. Ujvári, G. G. Láng, *Electrochem. Comm.* **2012**, *19*, 1–4.
4. S. Vesztergom, G. G. Láng, *J. Instrum. Sci. Technol.* **2013**, *41*, 82–95.
5. S. Vesztergom, M. Ujvári, G. G. Láng, *Electrochim. Acta* **2013**, *110*, 49–55.
6. S. Vesztergom, M. Ujvári, G. G. Láng ***in*** Y. Saito, T. Kikuchi (eds), *Voltammetry: Theory, Types and Applications,* Nova Science Publishers, New York, 2013.
7. W. J. Albery, *Trans. Faraday Soc.* **1966**, *62*, 1915–1919.
8. W. J. Albery, *Trans. Faraday Soc.* **1966**, *62*, 1920–1931.
9. M. L. Hitchman, W. J. Albery, *Electrochim. Acta* **1972**, *17*, 787–790.
10. I. Annergren, M. Keddam, H. Takenouti, D. Thierry, *Electrochim. Acta* **1971**, *41*, 1121–1135.
11. L. Kiss ***in*** Studies in Physical and Theoretical Chemistry, Elsevier, Amsterdam, 1988.
12. W. Zurilla, E. Yeager, Tech. Rep. № 23-AD-694951, Office of Naval Research, 1969.
13. B. Miller, S. Bruckenstein, *J. Electrochem. Soc.* **1970**, *117*, 1032–1039.
14. A. J. Bard, L. R. Faulkner, *Electrochemical Methods: Fundamentals and Applications*, Wiley, New York, 2001.
15. C. M. A. Brett, A. M. O. Brett, *Electrochemistry: Principles, Methods and Applications*, Oxford University Press, Oxford, 1993.
16. W. J. Albery, M. L. Hitchman, *Ring–disc electrodes*, Oxford University Press, Oxford, 1971.
17. М. Р. Тарасевич, Е. И. Хрущева, В. Ю. Филиновский, *Вращающийся дисковый электрод с кольцом*, Наука, Moscow, 1987.
18. K. B. Prater, A. J. Bard, *J. Electrochem. Soc.* **1970**, *117*, 210–213.
19. S. W. Feldberg, M. L. Bowers, F. C. Anson, *J. Electroanal. Chem.* **1986**, *215*, 11–28.
20. J. Farkas, L. Kiss, Á. Fóthi, *Acta Chim. Acad. Sci. Hun.* **1980**, *104*, 405–415.
21. D. Britz, *Digital Simulation in Electrochemistry*, Springer, Berlin–Heidelberg, 2005.
22. T. Kármán, *Z. Angew. Math. Mechanik* **1921**, *1*, 233–252.
23. A. C. Riddiford ***in*** P. Delahay, C. W. Tóbiás (eds), Advances in Electrochemistry and Electrochemical Engineering 4, Interscience, New York, 1966.
24. W. G. Cochran, *Math. Proc. Cambridge Phil. Soc.* **1934**, *30*, 365–375.
25. M. J. Honeychurch, Simulating Electrochemical Reactions with Mathematica, IBNH, St Lucia, 2004.
26. B. G. Higgins, H. Binous, Steady Flow over a Rotating Disk: von Kármán Swirling Flow. Wolfram Demonstrations Project (3rd June 2011). http://demonstrations. wolfram. com/SteadyFlowOverARotatingDisk/VonKarmanSwirlingFlow.

Povzetek

Z uporabo grafičnega programskega jezika LabVIEW™, proizvajalca National Instruments®, smo razvili digitalni simulacijski model, ki opisuje elektrokemijske procese ob rotirajoči elektrodi z diskom in obročem. Model upošteva možnost uporabe neodvisnega potenciala na obeh delovnih elektrodah, predpostavlja homogeno elektrodno reakcijo, a dopušča prostorske nehomogenosti na površinah delovnih elektrod. Predstavljamo glavne programske koncepte ter osnovno delovanje simulacijskega softvera. Izvedli smo več simulacij, na osnovi katerih smo ocenili natančnost simulacijskih izračunov.